Sphere-on-Pillar Optical Nano-Antennas

Xudong Cui[1,*], Zheng Fan[2], Xinyong Tao[3], Weihua Zhang[4], Daniel Erni[5], Xudong Fan[2], Xiaobin Zhang[6], and Lixin Dong[2,*]

[1]China Academy of Engineering Physics, Mianyang, Sichuan 621900, China
[2]Michigan State University, East Lansing, Michigan 48864, USA
[3]Zhejiang University of Technology, Hangzhou 310014, China
[4]EPFL Lausanne, CH-1015, Lausanne, Switzerland
[5]University of Duisburg-Essen, D-47048, Duisburg, Germany
[6]Zhejiang University, Hangzhou 310014, China
[*]Email: xudong.cui@uni-duisburg-essen.de, ldong@msu.edu

***Abstract*—We propose an optical nano-antenna consisting of a pair of sphere-on-pillar structures. Experiments show that the controlled fabrication of metallic nanospheres on the tip of carbon nanotubes (CNTs) is effective, and numerical investigation revealed that a pair of such structures are capable to convert free space radiation into an intense near-field; hence can function as an optical antenna. The fabrication process, electron-beam-induced bubbling (EBIB) and electromigration-based bubbling (EMBB), are based on nanofluidic mass delivery at the attogram scale using metal-filled CNTs. Under the irradiation of a high energy electron beam of a transmission electron microscope (TEM), the encapsulated metal is melted and extruded out from the tip of the nanotube; generating a metallic sphere. In the case that the encapsulated materials inside the CNT have a higher melting point than that of the beam energy can reach, electromigration-based mass delivery is an optional process to apply. Under a low bias (2-2.5V), spherical nanoparticles are formed on the tips of nanotubes. The optical properties of the nano-antenna are analyzed numerically using the finite element method. Our investigations have revealed that the field enhancement, the resonances, and the radiation patterns can be easily tuned since all these quantities strongly depend on the size of the nanotubes and the metallic spheres, as well as on their material properties. Sphere-on-pillar optical antennas carry a great potential for bio-sensing, tip-enhanced spectroscopy applications, and interfacing integrated nanophotonic circuits.**

Index Terms – Carbon nanotube, sphere-on-pillar nanostructure, optical antenna, nanofluidics, nanophotonics

I. Introduction

Optical antennas [1-3] can efficiently couple far-field radiation to a sub-wavelength sized near-field, provided the possibilities to tailor the optical properties of the underlying nanostructure. The feasibility of optical nano-antennas has been demonstrated in the context of enhanced single molecule light emission and absorption [2], field-enhanced spectroscopy [4], and nanolithography [5]. All these antenna structures are made of noble metals and thus the localized surface plasmon resonances are playing a central role in the optical responses of functional nanostructures, where the incident light is efficiently absorbed by the metallic nanostructure and/or redirected as scattered light at resonance. Due to the highly dispersive nature of the underlying material system, it becomes a major challenge to engineer such optical nano-antennas according to the desired specifications, not to mention the challenges that are faced in fabrication technology, such as material compatibility in composite nanodevices, as well as the difficulty to access experimental data from such nano-sized functional topologies. Moreover, these plasmonic nanostructures are quite sensitive with respect to the structure morphology and the surrounding environment [1-5]. Designs with controllable properties (materials, geometries etc.) either during fabrication or at the post processing stages are therefore anticipated to be capable of overcoming some of those difficulties. Besides noble metallic particles, carbon nanotubes (CNTs) have been demonstrated as nanooptical antennas [6, 7]. Nevertheless, the antenna effect in CNTs is not as pronounced as in its classical microwave counterpart because of the large material losses. Even though, CNTs provide an ideal system to study optical antennas because of their well-adapted shape, but also due to their tunable material properties [8]. Recently, copper-filled CNTs have been demonstrated for attogram level mass deposition and spot welding using nanorobotic manipulation [9]. We expect that such a combination of metallic parts with nanotubes would provide significant degrees of freedom to realize a new type of optical nano-antenna. Hence, we propose a dual-segmented optical nano-antenna (Fig. 1), where a pair of metallic spheres is bubbled onto the ends of CNTs.

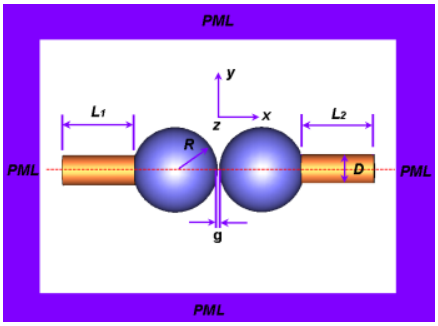

Fig. 1 Optical nano-antennas. The spheres are joint to two identical cylindrical parts ($L_1 = L_2$) to mimick the support provided by the corresponding nanotubes. The cylinder axes coincide while forming a direct connection between the centers of the two spheres. The computation window is truncated using perfectly matched layers (PMLs) to avoid spurious reflections.

II. Fabrications

A verity of techniques, such as inversed self-assembly grafting, wet-chemistry surface assembly, water-flow suction, photocatalytic deposition, and optical trapping, have been developed to attach metallic nanoparticles on a cantilever tip or an optical fiber [10], however, the controlled attachment of individual nanoparticles on nanopillars has been shown infeasible [10].

Here we propose two processes, electron-beam-induced bubbling (EBIB) and electromigration-based bubbling (EMBB), for the fabrication of the structures of nanospheres on pillars. The technique resembles blowing a balloon using a pipe and is technically based on nanofluidic mass delivery at the attogram scale using metal-filled carbon nanotubes (m@CNTs). In previous works, electron-beam-induced expansion, melting, and flowing of the encapsulated materials inside a nanotube have been observed, and potential applications such as thermometers and extruders have been demonstrated [11-13]. Investigations on the intra- and inter-nanotube mass melting, flowing, evaporation, and delivery based on electromigration [9, 14] have enabled new techniques such as nanorobotic spot welding [9] and devices such as archival memories [15]. Bubbling involves several novel aspects such as pressure accumulation inside nanotubes, nanotube tip breaking or opening, and shaping and sizing of the particles.

A. EBIB of Sn-filled CNTs

Sn-filled CNTs (Sn@CNTs) [13] were used to show the process of EBIB. The experiments were performed in a transmission electron microscope (TEM, JEOL 2200FS) with a field emission gun. In the experiments, individual Sn@CNTs were exposed under the high energy electron-beam. The current density of the electron beam transmitting through the CNTs was adjusted by changing the beam convergence as well as the magnification and the incident area. Figure 2 (a) to (j) show the formation of a Sn sphere on the tip of a CNT (The setup is schematically shown in Fig. 2 (k)) at a current density of 20 A/cm^2 with a magnification of ×300K and an irradiation area of 1.3×10^{-14} cm^2. In our previous investigations, we have observed melting and expansion of tin inside CNTs when the current density reached 0.4 A/cm^2 [13], here we observed that a bubbling process will follow (Fig. 2 (e) to (j)). At the beginning of the process, polyhedral nanoparticles (Fig. 2(g) and (h)) were formed. By increasing temperatures, they were developed into spheres (Fig. 2(j)) [16]. We attribute the bubbling and the shape conversion to the electron irradiation and the secondary effects including the carbon shell reconstruction and the surface tension of the molten metal. The encapsulated materials were melted and then squeezed out by the carbon shells as spheres onto the top of nanotubes. Applying an image processing method, the mass of the sphere is analyzed. The CNT has an external diameter of ~40nm. The diameter of the final sphere is 54 nm, and the mass of the resulted sphere is 0.6 fg (femtograms) according to the density of the tin (7.31 g/cm^3). The influence of the current densities on the formation speed and the diameter of the spheres are depicted in Fig. 2 (l).

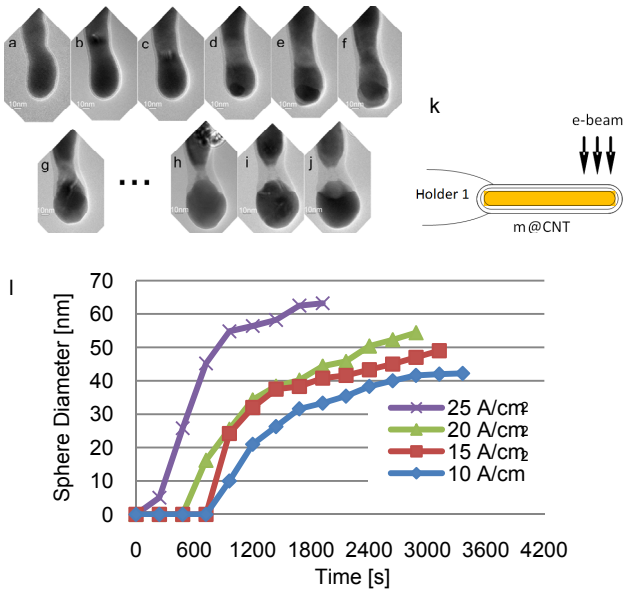

Fig. 2. Fabrication of sphere-on-pillar nanostructures using EBIB. (a) A Sn-filled CNT was brought to under the exposure of electron beam at t = 0s. (b, c) Under the current density of 20A/cm^2 from 240s to 480s, a molten section of tin appeared and moved to the tip of the tube, which deformed the tip of the tube into a quasi-spherical shape. (d) At t=720s, the inner metal first broke out from the tube. (e, f) Metal started to flow out. The carbon shell near the tip of tube was deformed more, which attributed to the squeezing out of the Sn sphere from the nanotube shell. (g) At t=1440s, a sphere is visible on the tip of the CNT. (h-j) The shape changed with time and a sphere was formed at t=2880s. The shrinkage of the carbon shell prevented more metal to flow from the bottom to the tip of the tube. (k) Schematic drawing of EBIB. (l) shows the influence of the current densities on the formation speed and the diameter of the spheres.

B. EMBB of Cu-filled CNTs

A scanning tunnelling microscope built in a TEM holder (Nanofactory Instruments AB) is adopted for EMBB. By delivering the encapsulated materials from the carbon shells, nanospheres are bubbled over the CNT tips (Fig. 3(a)).

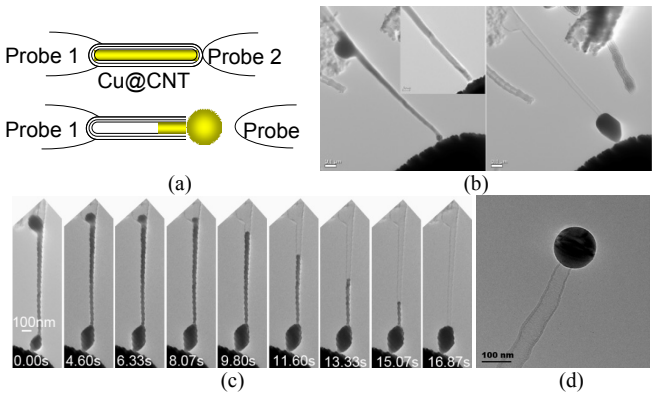

Fig. 3 Fabrication of sphere-on-pillar nanostructures using EBIB. (a) Schematic of the fabrication of spheres on CNTs by flowing out encapsulated metal from a nanotube using electromigration. (b) EMBB from a Cu-filled CNT. Inset shows that the nanotube has an opened cap originally. (c) Detailed series of (b). (d) A sphere formed on a CNT without an initial opening. The diameter of the sphere is $2R$ = 140 nm, and the diameter of the CNT D is about 50 nm.

During the experiments, the intensity of the electron beam has been kept in the range for regular imaging, which is several orders of magnitude lower than the above-mentioned values. Results show that under a low bias (2-2.5 V), spherical particles can be formed on the tip of nanotubes. At a low temperature, polyhedral nanoparticles (Fig. 3(b) and (c)) rather than spheres (Fig. 3(d)) will be formed. By increasing temperatures, it is possible to convert polyhedral nanoparticles into spheres.

III. Modeling and Simulations

The nano-antenna under consideration is displayed in Fig. 1, where a metallic sphere that is attached at the near end of the nanotube has been mirrored accordingly to form a paired nano structure ($L_1 = L_2$) with a feed gap. The feed gap g is initially selected to be 20 nm, which indicates the smallest distance between the two surfaces of spheres we could experimentally achieve. The entire structure is embedded in vacuum. Other structural parameters, such as the diameter of the two spheres and the dimensions of the joint nanotubes are adapted from our fabricated structure shown in Fig. 3(d). A plane wave incident from below [i.e. from the –y-direction, cf. Fig. 1] is used as excitation within a wavelength range from 400 nm up to 1200 nm. The polarization is chosen to be parallel to the axes of the nanotubes and the electric field strength amounts to $E_x = 1$ V/m. The simulations are carried out using the Finite Element Method (FEM) included in the COMSOL Multiphysics modeling platform. We adopt the FEM mainly for its compatibility with curved geometry due to its adaptive meshing capabilities. Meshing becomes particularly critical when dealing with structures with feature sizes differing in several orders of magnitude. Mesh sizes as small as 0.5 nm are used throughout the calculations when compared to the overall size of the antenna structure, resulting in $5\text{-}9\times10^5$ degrees of freedom (indicating the number of parameters required for the derived field in the simulation space). The field was calculated in the framework of the scattered field formulation by using perfectly matched layers (PMLs) to avoid spurious reflections from the surrounding medium boundaries [Fig. 1]. Since FEM is memory-hungry for 3D simulations, the direct solver PARDISO is used and the computation time for the paired geometry amounts to about 58-90 hours on an Intel quad-core processor (3 GHz) with 32 GB RAM.

From numerical considerations, a MWNT is usually set to be equivalent to a single-walled CNT (SWNT) with a much larger effective radius and an effective conductance [17]. For example, the complex dielectric function for an infinitely long SWNT is expressed as a function of effective conductance σ_{cn} and the frequency as follows:

$$\varepsilon_{cn}(\omega) = 1 + \frac{\sigma_{cn}}{j\omega\varepsilon_0}\cdot(S\cdot\rho_T) \tag{1}$$

Where ω is the angular frequency, ε_0 is the permittivity of free space, ε_{cn} is the complex dielectric function for the SWNT, S is the surface area of the nanotube and ρ_T is the volume density of the proper tube [18]. The effective conductance for an N-layer MWNT is then given by the simple relation $\sigma_{cn}^{M} = N\cdot\sigma_{cn}$. The effective radius of the MWNT is defined as $R_{eff} = R = (R_1 + R_2)/2$, where R_1 is the radius of inner wall and R_2 is the radius of the outer wall. It should be noted that the optical conductance could be varied, due to different factors that are affecting the electronic conductivity of SWNT, including the doping level of the semiconducting tubes, the sample purity, and the metal-to-semiconductor volume fraction [9, 19]. In addition, since the MWNTs basically consist of multi-layered concentrically aligned SWNTs, the intertube interactions should be taken into account with respect to the applied field polarizations [20]. Referring to the antenna application we expect an electric polarization, which is parallel to the tube axis. In this case, the intertube interactions play a less important role and can therefore be neglected in the simulations. This polarization direction also supports a significant field enhancement, while virtually no enhancement is evident when the electric field is not parallel to the axis of nanotube [cf. Fig. 1].

The nanotubes can either be metallic or semiconducting depending on the fabrication technology, which has a considerable influence on the resonant features of our antenna structures. For this reason, we will only discuss one specific case, namely a nanotube with a fixed dimensional size (tube radius) that is modeled as being metallic. The data for the nanotube used in the calculations is shown in Fig. 3(d). For the metallic spheres, we used measured data of silver according to the well-known reference of Johnson and Christy [21].

A. Optical properties of the paired structure

In this section, we investigate the optical properties of the nano-antenna as depicted in Fig. 1. The resulting computed spectral responses of the electric field in the center of the gap (antenna feed) is shown in Fig. 4(b) for different nanotube lengths and for a plane wave excitation with $E_x = 1$ V/m. For comparison, the spectral response of the antenna structure without nanotubes ($L_1 = L_2 = 0$) is displayed in the same figure. One resonance at 686 nm is identified for the sole paired sphere structure, with the corresponding field enhancement factor of 10.75 [cf. Fig. 4(b)]. The large field enhancement between the two spheres is attributed to near-field interactions that increase the surface charge density, and hence, the field strengths associated to the present surface plasmon (SP) modes at resonance [7]. The resonant field pattern of the structure ($L_1 = L_2 = 0$) at 686 nm is characterized as a fundamental dipole mode, based on the fact that the antenna response is maximized when the antenna length is an odd multiple p of half the effective wavelength λ_{eff} (i.e. $L = p\cdot\lambda_{eff}/2$, with $p = 1$ for the dipole mode) [4]. Note that due to material dispersion at optical frequencies, the effective wavelength of an optical antenna is usually very short and strongly material-dependent. An alternative way to identify the mode order of an antenna is to analyze the current distribution in the proper structure [19]. The resonant electric and magnetic field distributions for the sole paired structure without CNTs are shown in Fig. 4(c-d). As observed here, the fields primarily

concentrated in the gap region with maximal values in the gap center and die off toward both antenna ends. When the nanotubes ($L_1 = L_2 < 100$ nm) are added into the structure, the electric field in the gap increases at the resonant wavelengths compared with the sole paired structure. The field enhancement is also promising at shorter wavelength, i.e., in the wavelength range 300-550 nm. In general, the field increases [cf. Fig. 4(a)] for a nanotube length of $L_1 = L_2 < 500$ nm at shorter wavelengths. This further shows that the field enhancement is a function of the length of CNT, where the presence of CNT affects the charge density on the spheres, resulting in varied coupling strength within the gap. Another fact to be noted is that the field enhancement is associated with the material properties of both, silver and CNT, where the material losses are small at long wavelengths for both materials.

It is well known for plasmonic structures that the SP resonances strongly depend on the shape and size of the structure, as well as on the material losses [7]. A more efficient way to improve the field enhancement in our antenna topology is to increase the lightning rod effect by reducing the size of the metallic spheres while keeping a fixed gap width. This reduction can be realized by precisely controlling the parameters of the nanoscopic welding process [11], where the sphere can be made even as small as the diameter of the nanotube (~50 nm). An alternative scheme to increase the field enhancement in the gap also consists in altering the metallic doping level in the CNT fabrication to reduce the losses of CNT. Notably, the electric field in the gap drops exponentially with increasing gap size, indicating that small gap widths are necessary in order to keep a large field enhancement and, hence a high optical intensities in the antenna feed. A huge field enhancement in the gap is therefore observed for two nearly touching spheres [20]. However, it is nearly impractical to accurately assemble two spheres with such a small gap size (i.e. $g = 1$ nm or even less). Therefore, additional methods have to be applied to create such small gaps in order to generate so-called "hot spots" [5]. Hot spots, namely, large optical intensities are beneficial when exploiting nonlinear properties such as e.g. optical frequency mixing on metallic surfaces [22]. More exotic applications such as single-photon sources may be realized by placing individual quantum emitters inside the gap to enhance light-matter interactions [23].

The resonance shift of nano-antenna structures is also of interest, since the related effective antenna length is an important indicator of various antenna effects [19]. When the nanotubes are added to the spheres, the spectral resonances of the structure undergo a red-shift as shown in Fig. 4(b). For example, the introductions of a 50 nm-long nanotube gives rise to two resonances in the wavelength range of interest (400-900nm), which occurs at the wavelengths of 526 nm and 842 nm (the related field enhancement factors at these two resonances are 9.5 and 12.6, respectively). Compared to the fundamental resonance

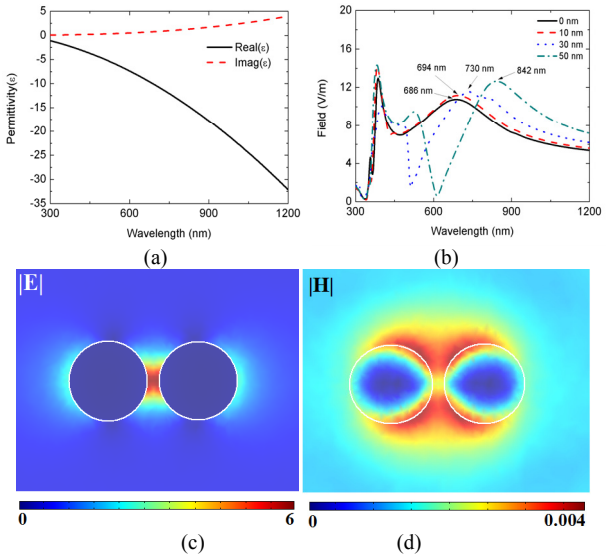

Fig. 4. (a) Permittivity of the MWNT as a function of wavelength used in our calculations; (b) Electric field strength in the center of the gap as a function of the wavelength for various MWNT lengths. Some of the resonant wavelengths for the paired structure are indicated with corresponding arrows. (c) Electric field distribution for the sole paired structure at the resonant wavelength of 686 nm; (d) Magnetic field distributions for the sole paired structure at the resonant wavelength of 686 nm. The red and bright colors in the figure indicate high field values.

of the sole paired silver sphere structure (at 686 nm), the fundamental resonance wavelength of the resulting nano-antenna (with $L_1 = L_2 = 50$ nm) is now red-shifted by 156 nm reaching a value of 842 nm. Increasing the length of the two nanotubes further (i.e., $L_1 = L_2 = 100$ nm, 200 nm), provides even larger red-shifts (~ 500 nm). The resonant mode appearing in the structure (with $L_1 = L_2 = 50$ nm) at 526 nm is identified as high-order dipole-like modes based on their current distributions within the structure and the associated radiation patterns. This additional resonance is significantly narrower than the fundamental one at 842 nm. It is even more interesting that the introduction of a 10 nm-long CNT would cause 8 nm resonance shift as shown in Fig. 4(b), implying that this type of multi-segmented structure might provide an efficient way to tune the resonance of plasmonic structures without increasing the structural size too much. In addition, only small resonance shifts are observed if the length of the nanotube becomes longer than several wavelengths (i.e., 5λ), while the size of both, the gap and silver sphere are kept unchanged ($g = 20$ nm, $R = 70$ nm). Some resonances – which remain nearly unchanged (i.e., shift less than 3 nm) when the CNTs are introduced to the structure – are observed at short wavelengths (at 378-381 nm). Our antenna structure is thus best suited for applications where small resonance shifts are beneficial, such as e.g. tip-enhanced applications. For instance, negligible small resonance shifts can inhibit the spectral mismatch between the laser source and the tip resonance if the structure is properly designed. Further numerical studies have revealed that the size of spheres and the gap width are the most relevant geometric parameters for tuning the resonance based on the configuration shown in Fig. 1: some

resonances will red-shift while increasing the gap size and finally leak out from the wavelength range of interest, rendering the spheres more and more uncoupled. These findings comply well with similar studies on pure metallic bow-tie antennas [24] and dimer plasmonic antennas [14].

B. Radiation Properties

From the above investigations, we can see that the added CNTs do have a strong influence on the field enhancement, as well as on the resonance of the structure. The antenna effects associated to the nanowires are arising from photon confinement in the structures, where internal standing wave photon modes are generated in the wire under proper light illumination [25]. It is well-known from antenna theory that antennas radiate from currents and while tailoring the current distribution in the structure enables to design a desired radiation pattern [19]. Therefore, currents in antennas play an important role on the antenna effects. Figure 5(a) shows the magnetic field distributions at three resonance wavelengths of the structure with two 200 nm nanotubes. Note that the corresponding current distribution can be obtained when integrating the magnetic field over the antenna surface. At the resonance wavelength of 382 nm the dominant field strength is found in the gap (i.e. the antenna feed) and the field distributions at the two joints and the CNT are barely visible; while at the resonance wavelengths of 568 nm and 708 nm, the fields are predominantly distributed on the CNT arms and the gap regions. This implies that the interacting fields between the two antenna arms can vary as a function of the excitation wavelength. We also plot the normalized magnetic field strength along the antenna axis. At each resonance it displays a sort of alternating modulation across the structure [cf. Fig. 5(b)], which gets more pronounced for shorter wavelength and shorter CNTs. Nevertheless, this field modulation will become weaker if both CNTs yield a length larger than the wavelength (e.g. 5λ). An increasing length is obviously associated with a red-shift of the aforementioned resonance, where the wavelength shift becomes small if the CNTs are both exceeding the aforementioned limit of 5λ.

Above facts imply that the presence of the CNTs may impact the radiation properties, despite the antenna effect of CNT itself is relatively weak due to high material losses [8]. In order to validate the influence of CNT on the emission characteristics, we numerically investigated the radiation patterns at the corresponding resonances of the antenna structure. The radiation patterns are obtained for the upper half x-0-y plane [i.e. the E-plane as indicated in Fig. 1]. The radiation characteristics in Fig. 6(a) are displayed for the sole paired sphere structure without the two CNTs. The resonance at 686 nm is maintained by the dipole-like fundamental mode; while some other resonance such as e.g. the one at 386 nm has a multipole high-order mode pattern, with a main lobe having a beamwidth of around 30°. This multipolar nature of the emission pattern owes to the frequency dependence of the near-field coupling as well as

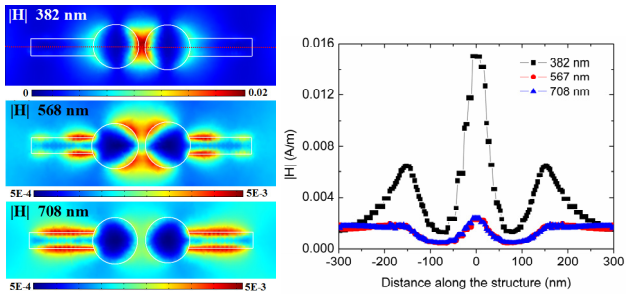

(a) (b)

Fig. 5. (a) Distribution of the magnetic field strength in the antenna structure with two 200 nm nanotubes at two different resonances. The unit used in the color bar is A/m; (b) Magnetic field strength along the axis of the structure at the two resonances; the axis is indicated as the dashed line shown in Fig. 5(a).

to the fact that the minor lobes are arising from the spectrally varying charge distributions at the far-end of the antenna topology. Therefore, it is not surprising that the main and minor lobes of the far-field characteristics have different beamwidths as shown in Fig. 6 due to the different bandwidths of the corresponding resonances. More interestingly, different modes show correspondingly different radiation efficiencies. For example, the far-field radiation is stronger at 386 nm than at 686 nm [cf. Fig. 6(a)], where a stronger field enhancement was found at 386 nm. When two 50 nm CNTs are introduced into the structure, minor lobes still appear in the radiation patterns [cf. Fig. 6(b)] but with different beam widths and field strengths compared to the radiation patterns of the bare sphere structure [cf. Fig. 6(a)]. However, the bandwidth differences for the multipolar modes are graphically indistinguishable from the comparison between Fig. 6(a) and Fig. 6(b), since the resonance bandwidths are only slightly different at those resonances. For the dipolar modes, the bandwidth difference is graphically discerned, due to the improved suppression of the minor sidelobes, which are originating from multiple mode interactions with the far-end of both, the metallic parts and the CNT parts. As the nano-antenna is operated in a distinct sub-wavelength regime the minor lobes can be further suppressed by increasing the length of CNT; or then by optimizing the overall antenna shape. Both measures are

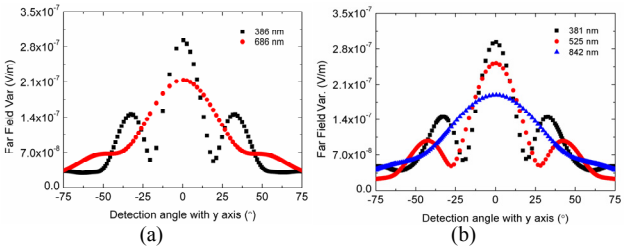

(a) (b)

Fig. 6. Far-field radiation characteristics of the structure with respect to the x-y-plane (E-plane): (a) Two spheres without CNTs at resonance wavelengths of 386 nm and 686 nm, the mode at 386nm is characterized as multipolar mode, the mode at 686 nm is dipole-like mode; (b) Two spheres with two 50 nm long semiconductor CNTs at the resonant wavelengths of 381 nm, 525 nm (multipolar mode) and 842 nm (dipole-like mode), respectively. The relevant dimensions of the two spheres are R = 70 nm and g = 20 nm.

equivalent to the tailoring of the current flow in the proper structure, which actually corresponds to a well-established strategy in RF antenna design [19]. In addition, the narrowing in beam width that comes along with the sidelobe suppression in the structure owes definitely to the CNT antenna effect, which refers to the current modulations in both antenna arms. The antenna performance can thus be further improved by reducing the radius of both, the CNT and the sphere. Due to the increased field enhancement, higher radiation field strength together with a correspondingly tailored radiation pattern can be obtained.

IV. Conclusions

In conclusion, we proposed a new type of optical antenna that encompasses a pair of sphere-on-pillar nanostructure. EBIB and EMBB have been shown effective for the fabrications of nanospheres on nanopillars. EBIB does not need to make a contact of the nanotube to an electrode; hence featured with simplicity. However, the process is time-consuming and involves high energy beam. To the materials with a high melting point, EMBB is a method to be applied. The copper-filled CNTs in the experiment has a 40-nm diameter, and the flowing has continued for 17 s at the flow rate of 82.3 nm/s and the bias threshold for the flowing is 2.4 V. The sphere-on-pillar optical antenna has proven successful to interrelate free space radiation with intense near fields in the feed point addressing both, the aspect as receiving antenna as well as the characteristics of the nano-emitter. The antenna resonances, the associated field enhancement, as well as the radiation pattern can be efficiently tuned since they strongly vary with respect to structural parameters like the length and the material properties of the nanotubes, the size of the spheres, and the gap size. It is worth noting that the proposed antenna design is not restricted to the materials we used here. Other noble metals, such as gold, copper are applicable to yield different antenna performance. Since our nanostructure can be precisely tailored during fabrication and post-processing stages, the remarkable tuning properties allow us to promote it as a highly efficient optical nano-antenna with tailored radiation characteristics applicable to the various fields in the realm of functional nano-optics.

References

[1] P. Muhlschlegel, H. J. Eisler, O. J. F. Martin, B. Hecht, and D. W. Pohl, "Resonant optical antennas," *Science,* vol. 308, pp. 1607-1609, Jun 2005.

[2] J. J. Greffet, "Nanoantennas for light emission," *Science,* vol. 308, p. 1561, Jun 2005.

[3] L. Novotny, "Effective wavelength scaling for optical antennas," *Physical Review Letters,* vol. 98, art. no. 266802, Jun 2007.

[4] J. Aizpurua, G. W. Bryant, L. J. Richter, F. J. G. de Abajo, B. K. Kelley, and T. Mallouk, "Optical properties of coupled metallic nanorods for field-enhanced spectroscopy," *Physical Review B,* vol. 71, art. no. 235420, Jun 2005.

[5] A. Sundaramurthy, P. J. Schuck, N. R. Conley, D. P. Fromm, G. S. Kino, and W. E. Moerner, "Toward nanometer-scale optical photolithography: Utilizing the near-field of bowtie optical nanoantennas," *Nano Letters,* vol. 6, pp. 355-360, Mar 2006.

[6] K. Kempa, J. Rybczynski, Z. P. Huang, K. Gregorczyk, A. Vidan, B. Kimball, J. Carlson, G. Benham, Y. Wang, A. Herczynski, and Z. F. Ren, "Carbon nanotubes as optical antennae," *Advanced Materials,* vol. 19, pp. 421-426, Feb 2007.

[7] J. Rybczynski, K. Kempa, Y. Wang, Z. F. Ren, J. B. Carlson, B. R. Kimball, and G. Benham, "Visible light diffraction studies on periodically aligned arrays of carbon nanotubes: Experimental and theoretical comparison," *Applied Physics Letters,* vol. 88, art. no. 203122, May 2006.

[8] P. Avouris, Z. H. Chen, and V. Perebeinos, "Carbon-based electronics," *Nature Nanotechnology,* vol. 2, pp. 605-615, Oct 2007.

[9] L. X. Dong, X. Y. Tao, L. Zhang, X. B. Zhang, and B. J. Nelson, "Nanorobotic spot welding: Controlled metal deposition with attogram precision from copper-filled carbon nanotubes," *Nano Letters,* vol. 7, pp. 58-63, Jan. 2007.

[10] Y. Gan, "A review of techniques for attaching micro- and nanoparticles to a probe's tip for surface force and near-field optical measurements," *Review of Scientific Instruments,* vol. 78, art. no. 081101, Aug 2007.

[11] Y. H. Gao and Y. Bando, "Carbon nanothermometer containing gallium - Gallium's macroscopic properties are retained on a miniature scale in this nanodevice," *Nature,* vol. 415, p. 599, Feb 2002.

[12] L. Sun, F. Banhart, A. V. Krasheninnikov, J. A. Rodriguez-Manzo, M. Terrones, and P. M. Ajayan, "Carbon nanotubes as high-pressure cylinders and nanoextruders," *Science,* vol. 312, pp. 1199-1202, May 2006.

[13] X. Y. Tao, L. X. Dong, W. K. Zhang, X. B. Zhang, J. P. Cheng, H. Huang, and Y. P. Gan, "Controllable Melting and Flow of β-Sn in Flexible Amorphous Carbon Nanotubes," *Carbon,* vol. 47, pp. 3122-3127, Nov. 2009.

[14] L. X. Dong, X. Y. Tao, M. Hamdi, L. Zhang, X. B. Zhang, A. Ferreira, and B. J. Nelson, "Nanotube fluidic junctions: Inter-nanotube attogram mass transport through walls," *Nano Letters,* vol. 9, pp. 210-214, Jan 2009.

[15] G. E. Begtrup, W. Gannett, T. D. Yuzvinsky, V. H. Crespi, and A. Zettl, "Nanoscale reversible mass transport for archival memory," *Nano Letters,* vol. 9, pp. 1835-1838, May 2009.

[16] X. D. Feng, D. C. Sayle, Z. L. Wang, M. S. Paras, B. Santora, A. C. Sutorik, T. X. T. Sayle, Y. Yang, Y. Ding, X. D. Wang, and Y. S. Her, "Converting ceria polyhedral nanoparticles into single-crystal nanospheres," *Science,* vol. 312, pp. 1504-1508, Jun 2006.

[17] J. Hao and G. W. Hanson, "Optical scattering from a planar array of finite-length metallic carbon nanotubes," *Physical Review B,* vol. 75, art. no. 165416, Apr 2007.

[18] J. Zhou, T. Koschny, M. Kafesaki, E. N. Economou, J. B. Pendry, and C. M. Soukoulis, "Saturation of the magnetic response of split-ring resonators at optical frequencies," *Physical Review Letters,* vol. 95, art. no. 223902, Nov 2005.

[19] C. A. Balanis, *Antenna Theory: Analysis and Design*. New York: Wiley, 2005.

[20] I. Romero, J. Aizpurua, G. W. Bryant, and F. J. G. de Abajo, "Plasmons in nearly touching metallic nanoparticles: singular response in the limit of touching dimers," *Optics Express,* vol. 14, pp. 9988-9999, Oct 2006.

[21] P. B. Johnson and R. W. Christy, "OPTICAL-CONSTANTS OF NOBLE-METALS," *Physical Review B,* vol. 6, pp. 4370-4379, 1972.

[22] M. Danckwerts and L. Novotny, "Optical frequency mixing at coupled gold nanoparticles," *Physical Review Letters,* vol. 98, art. no. 026104, Jan 2007.

[23] E. Peter, P. Senellart, D. Martrou, A. Lemaitre, J. Hours, J. M. Gerard, and J. Bloch, "Exciton-photon strong-coupling regime for a single quantum dot embedded in a microcavity," *Physical Review Letters,* vol. 95, art. no. 067401, Aug 2005.

[24] D. P. Fromm, A. Sundaramurthy, P. J. Schuck, G. Kino, and W. E. Moerner, "Gap-dependent optical coupling of single "Bowtie" nanoantennas resonant in the visible," *Nano Letters,* vol. 4, pp. 957-961, May 2004.

[25] G. Chen, J. Wu, Q. J. Lu, H. R. H. Gutierrez, Q. Xiong, M. E. Pellen, J. S. Petko, D. H. Werner, and P. C. Eklund, "Optical antenna effect in semiconducting nanowires," *Nano Letters,* vol. 8, pp. 1341-1346, May 2008.